Insertion of MoO_3 in Borophosphate Glasses Investigated by Magnetic Resonance Spectroscopies

G. Tricot,*[,†] K. Ben Tayeb,[†] L. Koudelka,[‡] P. Mosner,[‡] and H. Vezin[†]

[†]LASIR UMR-CNRS 8516, Université de Lille1, Lille, Villeneuve d'Ascq C5-59655 France

[‡]Department of General and Inorganic Chemistry, University of Pardubice, Faculty of Chemical Technology, Pardubice 53210, Czech Republic

ABSTRACT: Insertion of MoO_3 oxide in the mixed borophosphate glass network has been analyzed for the first time by advanced magnetic resonance spectroscopies. For the first time, the xMoO$_3$-(100-x)(50PbO-10B$_2$O$_3$-40P$_2$O$_5$) composition line has been investigated by 1D (^{11}B, ^{31}P, ^{95}Mo) and 2D-correlation NMR (^{11}B DQ-SQ, ^{11}B(^{31}P) D-HMQC) at high magnetic field (18.8 T). The set of data allowed for analyzing both local and medium range orders and identifying the modifications in the BOB and/or BOP mixing induced by the MoO_3 insertion. In a second step, continuous wave EPR has been used to detect the presence of Mo^{5+} ions, resulting from partial reduction of Mo^{6+} during the melting stage, and the chemical environment around the Mo^{5+} species has been documented for the first time by pulsed EPR technique (HYSCORE). Altogether, the data contribute to a better understanding of the glass network modifications induced by the MoO_3 insertion, including the nonlinear evolution of the glass transition temperature that has been explained by a modification of the glass network nature.

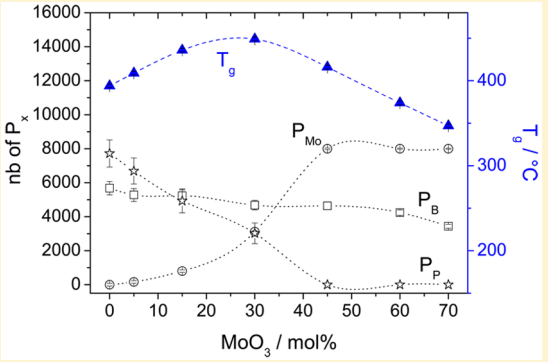

1. INTRODUCTION

Compared to classic silicate glass matrix, the high electrostatic field strength (z/a^2) of P^{5+} allows incorporating various oxides in high quantities in phosphate glasses.[1,2] This advantage of P_2O_5 over SiO_2 based glasses is well illustrated by the incorporation of molybdenum oxide. In silicate or borosilicate glasses, MoO_3 amounts higher than 3 mol % induce phase separation or crystallization,[3,4] whereas MoO_3 can be incorporated in homogeneous phosphate glasses up to 80 mol %.[5,6] Therefore, many studies have been devoted to MoO_3-containing phosphate based glasses over the last decades.[5−9] It has been shown that MoO_3 improves the glass thermal stability without inducing a significant increase of the glass transition temperature (T_g).[8,9] As already observed for other transition metal containing phosphate glasses, partial reduction of molybdenum occurs during the melting stage. The proportion of reduced species Mo^{5+} (defined as the glass redox = Mo^{5+}/Mo_{total} in our case) is controlled by the melting temperature/time/atmosphere or the melt optical basicity. While MoO_3-phosphate systems are known for their poor chemical durability, it has been shown that B_2O_3 insertion overcomes this limitation, leading to top quality and durable glass systems.[10−13] Numerous studies have been devoted to the characterization of the macroscopic properties of MoO_3 borophosphate glasses, but only sparse information is available on the glass network organization. No clear model has been proposed so far on the exact effect of molybdenum ions on the mixed borophosphate network. Vibrational and 1D NMR spectroscopies have recently been employed but do not afford clear results because of the complex Raman and NMR spectra assignment.[12,13] In this paper, new insights are provided by a magnetic resonance investigation performed on the xMoO$_3$-(100-x)(50PbO-10B$_2$O$_3$-40P$_2$O$_5$) composition line. Solid state ^{31}P, ^{11}B, and ^{95}Mo nuclear magnetic resonance (NMR) experiments have been used for the first time to analyze the local orders of the phosphate, borate, and molybdate units. Correlation NMR methods have been used in a second time to probe the ^{11}B/^{31}P and the ^{11}B/^{11}B interaction in order to detect the modifications in the POB and BOB connectivity. In addition, Mo^{5+} species have been characterized for the first time by continuous wave- (CW) and pulsed-electronic paramagnetic resonance (EPR) techniques. Unreported data about the chemical environment of the Mo^{5+} species have been derived from this work. Altogether, the set of data has been used to build a comprehensive structural model taking into account both oxidation states of the molybdenum element. A clear relationship between the glass transition temperature and the nature of the phosphate blocks has been established.

2. EXPERIMENTAL SECTION

2.1. Glasses Preparation and Characterization. Glasses have been prepared in the xMoO$_3$-(100-x)(50PbO-10B$_2$O$_3$-40P$_2$O$_5$) composition line with the standard melt-quenching procedure. Appropriate mixtures of analytical grade PbO,

MoO_3, H_3BO_3 and H_3PO_4 have been mixed, placed in a platinum crucible, calcined up to 600 °C for 2 h, and heated up to 1000−1350 °C for 20 min. The melts have been finally poured into a preheated graphite mold to obtain glasses that have been annealed 2 h at a temperature 5 °C below T_g. The amorphous character has been checked by X-ray diffraction experiments (not shown here). Volatilization losses appear to be minor, and the glass compositions have been referred to the batch compositions. The glass transition temperatures T_g have been measured using a DTA 404PC operating in DSC mode on 100 mg powder under N_2 atmosphere and at a 2 K/min heating rate.

2.2. NMR Analyses. The ^{31}P, ^{11}B, and ^{95}Mo MAS NMR experiments have been performed on a 18.8 T AVANCE-III Bruker spectrometer at 324.1, 256.8, and 49.2 MHz, respectively. The ^{11}B and ^{31}P (and ^{95}Mo) experiments have been performed at a spinning frequency (ν_{rot}) of 20 kHz using prototype B/P- (and standard HX-) 3.2 mm probeheads, respectively. The 1D ^{31}P NMR acquisitions have been recorded using 1.7 μs pulse length (30° pulse angle), 32 transients and a 120 s recycle delay (rd); the 1D ^{11}B NMR spectra have been acquired with a 0.7 μs pulse length (10° angle pulse), 64 transients and a 4 s rd. The 1D Q-CPMG[14,15] ^{95}Mo experiments have been recorded using 20−30 k transients and 2 s rd. The ^{31}P, ^{11}B, and ^{95}Mo chemical shifts are referred to H_3PO_4, BF_3-Et_2O, and Na_2MoO_4 solutions as 0 ppm, respectively.

The medium range order of the borophosphate network has been analyzed using the $^{11}B(^{31}P)$ *Dipolar* Heteronuclear Multiple Quantum Coherence (*D*-HMQC)[16,17] and ^{11}B Double Quantum-Simple Quantum (DQ-SQ)[18] NMR techniques. The $^{11}B(^{31}P)$ *D*-HMQC spectra have been recorded using 10 and 5 μs 90° pulses length on ^{11}B and ^{31}P channel, a $SR4^2_1$ recoupling scheme[19] of 2 ms, 2474 (t2) × 50 (t1) acquisition points, and a rotor-synchronized t1 increment (50 μs). Each t1 slice has been recorded using 256−512 accumulations and 3 s rd. The 2D $^{11}B/^{31}P$ maps obtained here trace the B/P spatial proximity and can be used to determine the B/P connectivity scheme, as recently shown in case of alkali borophosphate systems.[20] The interactions between the different borate units have been investigated with the DQ-SQ technique. The 2D spectra were recorded using 2048 (t2) × 150 (t1) acquisition points with a 17 μs 180° pulse length, an excitation/conversion times of 200 μs using the $BR2^1_2$ pulse scheme,[18] 64 transients separated by a rd of 4 s and a rotor-synchronized t1 increment time of 50 μs. The 2D maps obtained here will be used to discuss the BOB linkage presence and nature.

2.3. EPR Analyses. CW-EPR spectra have been recorded at room temperature with a Bruker ELEXSYS E500 spectrometer operating in X band (9.5 GHz) with 0.63 mW microwave power, 5 G modulation amplitude, 82 s sweep time, and a time constant of 20.48 ms. Hyperfine interactions with ^{10}B, ^{11}B, ^{207}Pb, and ^{31}P nuclei have been studied at 5 K by pulsed EPR with a Bruker ELEXSYS E580 spectrometer equipped with a helium flow cryostat. 2-pulses echo field sweep acquisitions have been performed using standard Hahn echo sequence 90-τ-180- with 90 pulse length of 16 ns and τ value of 200 ns. The hyperfine sublevel correlation spectroscopy (HYSCORE)[21] experiments have been recorded with 256 × 256 data points, 90° pulse length of 16 ns, and an echo delay of 136 ns optimized with a 2D-3Pulses- electron spin echo envelop modulation (ESEEM).[22] The obtained HYSCORE spectra are composed of two quadrants: the first quadrant (+,−) where $A > 2\nu_I$ (ν_I being the nuclear frequency) corresponding to strong hyperfine coupling A between the I nucleus and the unpaired electron and the second quadrant (+,+) where $A < 2\nu_I$ corresponding to weaker interactions.

3. RESULTS

3.1. Glass Preparation and Characterization. Homogeneous and amorphous materials have been obtained in the $x$$MoO_3$-(100-$x$)(50PbO-10$B_2O_3-40P_2O_5$) composition line up to x = 70, confirming thus the ability of phosphate melts to incorporate high amounts of molybdenum oxide. The T_g evolution reported in Figure 1 can be decomposed in two domains: in low MoO_3 domain ($0 \le x \le 30$), T_g increases from 396 to 449 °C, whereas in the high MoO_3 domain ($x \ge 30$), T_g experiences a significant decrease down to 349 °C.

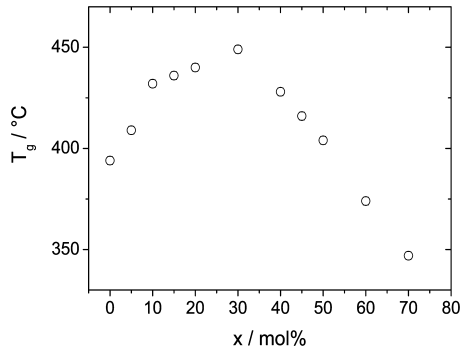

Figure 1. evolution of the glass transition temperature (T_g) in the $x$$MoO_3$-(100-$x$)(50PbO-10$B_2O_3-40P_2O_5$) glass series.

3.2. 1D MAS NMR Characterization. The ^{95}Mo Q-CPMG NMR experiments performed on representative compositions are presented in Figure 2. Broad signals centered around −100 ppm can be observed all along the composition line. If no significant evolution of the chemical shift can be observed, then a clear increase of the signal broadness occurs for MoO_3 contents higher than 30 mol %. The chemical shift values are close to the one previously observed in the $NaPO_3$−MoO_3

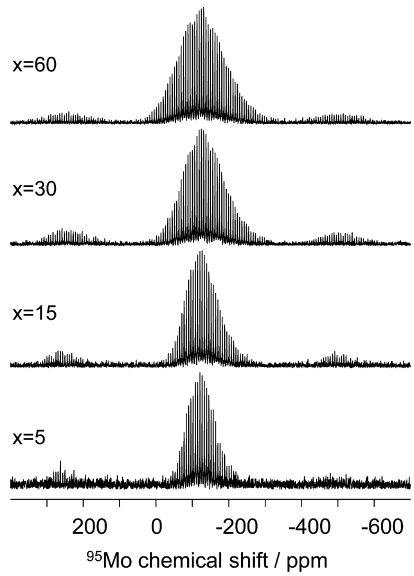

Figure 2. ^{95}Mo Q-CPMG NMR spectra of the $x$$MoO_3$-(100-$x$)(50PbO-10$B_2O_3-40P_2O_5$) glass series.

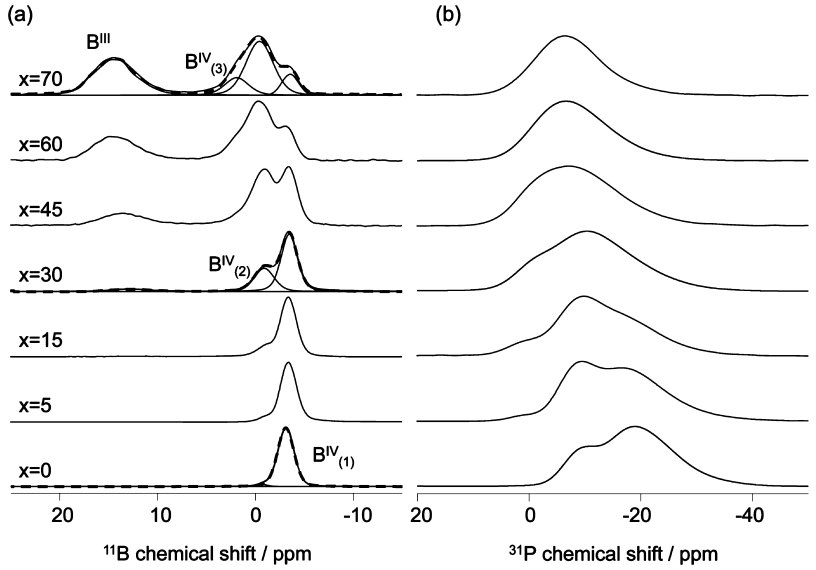

Figure 3. ^{11}B (a) and ^{31}P (b) MAS NMR obtained at 18.8 T on the xMoO$_3$-(100-x)(50PbO-10B$_2$O$_3$-40P$_2$O$_5$) glass series.

Table 1. ^{11}B NMR Parameters: Chemical Shift (δ_{iso}, ± 0.1 ppm), Full Width at Half Maximum (FWHM, ± 0.2 ppm), Quadrupolar Constant (C_Q, ± 0.1 MHz), Asymmetry Parameter (η_Q, ± 0.1), and Relative Proportions (Rel. Prop., ± 2%)

MoO$_3$ (mol %)	B^{IV}	δiso (ppm)	fwhm (ppm)	rel. prop. (%)	B^{III}	δiso (ppm)	C_Q (MHz)	η_Q	rel. prop. (%)
0	$B^{IV}_{(1)}$	−3.2	2.0	98	B^{III}				
	$B^{IV}_{(2)}$	−0.8	1.5	2					
5	$B^{IV}_{(1)}$	−3.4	1.9	95	B^{III}				
	$B^{IV}_{(2)}$	−0.9	1.5	5					
15	$B^{IV}_{(1)}$	−3.2	2.0	83	B^{III}	15.4	2.8	0.6	2
	$B^{IV}_{(2)}$	−0.8	1.5	15					
30	$B^{IV}_{(1)}$	−3.5	2.0	62	B^{III}	16.1	2.8	0.6	8
	$B^{IV}_{(2)}$	−0.9	2.4	30					
45	$B^{IV}_{(1)}$	−3.5	2.0	29	B^{III}	16.7	2.8	0.6	21
	$B^{IV}_{(2)}$	−0.9	2.7	41					
	$B^{IV}_{(3)}$	1.3	2.8	9					
60	$B^{IV}_{(1)}$	−3.4	2.1	15	B^{III}	17.9	2.8	0.6	34
	$B^{IV}_{(2)}$	−0.6	2.9	39					
	$B^{IV}_{(3)}$	2.1	2.8	12					
70	$B^{IV}_{(1)}$	−3.6	2.2	9	B^{III}	17.7	2.8	0.6	46
	$B^{IV}_{(2)}$	−0.7	3.1	33					
	$B^{IV}_{(3)}$	1.9	2.9	12					

system,[9] suggesting that Mo^{6+} species are present as 4-coordinated molybdate species. The 1D ^{11}B and ^{31}P MAS NMR spectra are reported in Figure 3. Owing to the high static magnetic field used in our experiments, the ^{11}B NMR analysis (Figure 3a) present resolved and separated regions corresponding to trigonal (B^{III}: 20/5 ppm) and tetragonal (B^{IV}: 5/−5 ppm) species, respectively. A single B^{IV} signal (denoted as $B^{IV}_{(1)}$) can be observed at −3.2 ppm for the based sample (x = 0). This signal has been observed in many publications[23−27] and is generally assigned to tetragonal boron attached to 4 P species. Introduction of MoO$_3$ oxide leads to a significant modification of the borate network with the progressive appearance of a second and third B^{IV} signals ($B^{IV}_{(2)}$ at 0.8 ppm and $B^{IV}_{(3)}$ at 1.5 ppm) and of a B^{III} resonance at 15 ppm. The ^{11}B spectra have been decomposed with the dmfit software[28] using Gaussian and quadrupolar models for the B^{IV} and B^{III} signals, respectively. The extracted parameters (isotropic chemical shift (δ_{iso}), full width at half-maximum (fwhm), Quadrupolar constant (C_Q), asymmetry parameter (η_Q)), and the relative proportions) are gathered in Table 1. Figure 4 presents the B^x site relative proportion evolutions and

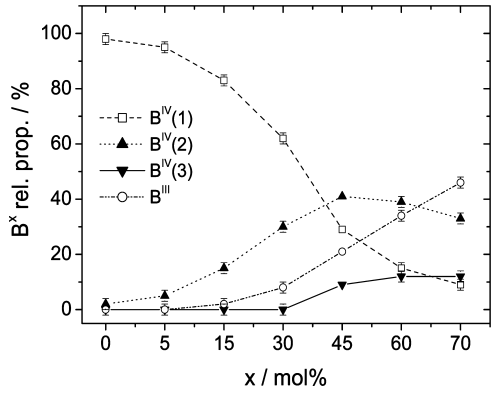

Figure 4. Evolution of the borate speciation in the xMoO$_3$-(100-x)(50PbO-10B$_2$O$_3$-40P$_2$O$_5$) glass series.

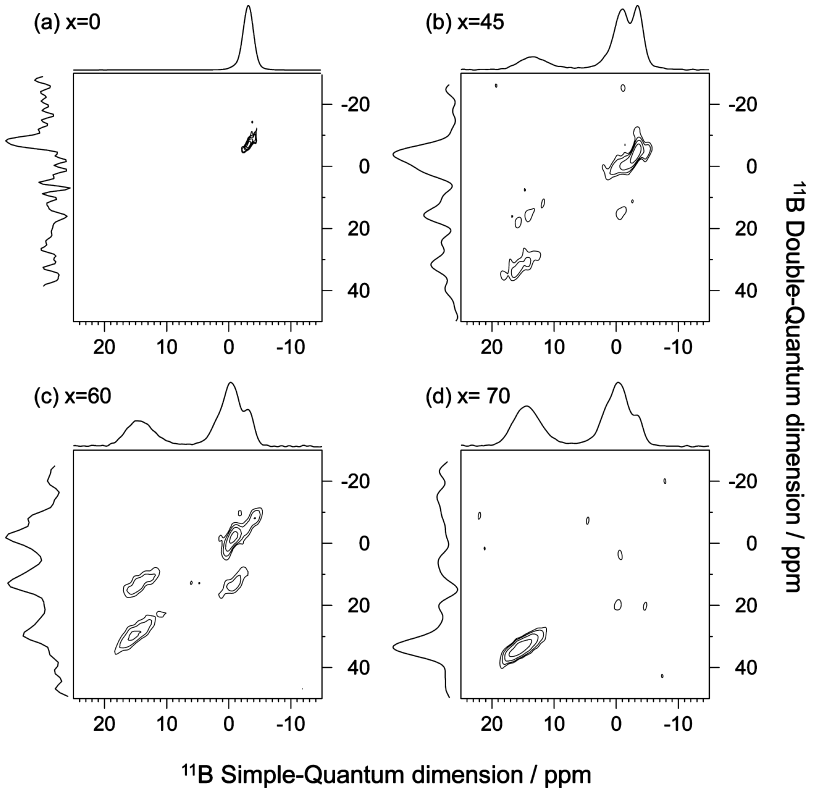

Figure 5. ^{11}B DQ-SQ 2D spectra of the x = 0 (a), 45 (b), 60 (c), and 70 (d) samples of the xMoO$_3$-(100-x)(50PbO-10B$_2$O$_3$-40P$_2$O$_5$) glass series. The 2D maps are displayed with the 1D ^{11}B MAS NMR spectrum and the 2D map double quantum projection on the horizontal and vertical axis, respectively.

shows that MoO_3 insertion leads to the decrease of $B^{IV}_{(1)}$ at the expense of $B^{IV}_{(2)}$ in the 0−30 mol % region and to the appearance and increase of B^{III} and $B^{IV}_{(3)}$ species in the 30−70 mol % region, these two latter units replacing the two previous species ($B^{IV}_{(1)}$ and $B^{IV}(2)$) at high MoO_3 amounts. The ^{31}P MAS NMR spectra are presented in Figure 3b. As expected in mixed glass network phosphate compositions,[23−30] the ^{31}P analysis present very broad signals, coming from the superimposition of several resonances with close chemical shifts. While the slight deviation of the global chemical shift toward positive values may be interpreted as evidence for phosphate network depolymerization, careful and supported analysis of the presented ^{31}P NMR data requires additional information provided by correlation NMR.

3.3. Correlation MAS NMR Characterization. The ^{11}B/^{11}B dipolar interactions are analyzed in Figure 5 through the edition of ^{11}B/^{11}B 2D maps in which correlation signals indicate short B—B distances that can be reasonably discussed in terms of BOB linkages. As observed in Figure 5a, the based composition (x = 0) presents a weak correlation signal, indicating that $B^{IV}_{(1)}$ slightly interacts with other $B^{IV}_{(1)}$ units to create BOB linkages. As previously reported,[26,27] the $B(OP)_4$ attribution generally admitted can thus be rediscussed and replaced by a $B(OX^{IV})_4$ assignment with X = P, B. At higher MoO_3 contents (x = 45), the 2D map (Figure 5b) indicates BOB mixing through the presence of on-diagonal $B^{IV}_{(1)}/B^{IV}_{(1)}$, $B^{IV}_{(2)}/B^{IV}_{(2)}$, and B^{III}/B^{III} signals accompanied by low intensity off-diagonal $B^{IV}_{(2)}/B^{III}$ signals. It is noteworthy that the B^{III}/B^{IV} signal only involves the $B^{IV}_{(2)}$ sites. Similar scheme can be observed for the x = 60 sample (Figure 5c) with more intense B^{III}/B^{IV} correlation signals, indicating a larger extent of B^{III}/B^{IV} mixing. At x = 70 (Figure 5d), only B^{III}/B^{III} signal can be observed without any trace of B^{IV}/B^{IV} or B^{IV}/B^{III} correlation. Presence of B^{IV} in significant amounts in the 1D MAS NMR analysis (Figure 5d, horizontal projection) of this sample indicates a strong simplification of the borate network structure and the presence of isolated 4-coordinate units. The interactions between borate and phosphate groups are analyzed in Figure 6 through the edition of ^{11}B/^{31}P 2D maps. As shown in Figure 6a, the presence of $POB^{IV}_{(1)}$ linkage is highlighted in the x = 0 sample through the presence of intense correlation signal. This structural features remains in the MoO_3 bearing compositions but is accompanied by $POB^{IV}_{(2)}$, $POB^{IV}_{(3)}$ and also POB^{III} correlation signals in Figure 6b−d, indicating that the four borate species are involved in the formation of mixed borophosphate linkages. The ^{31}P 2D map projections, showing the phosphate species involved in POB bonds, are gathered in Figure 7a and have been decomposed using a minimum number of components. The projection of the x = 0 sample reveals the presence of two main phosphate species connected to B^{3+} ions at −16.8 and −25.2 ppm, accompanied by a low intensity resonance at −6.0 ppm. The intense site (−16.8 ppm) can be assigned to a Q^1_{1B} unit (a phosphate connected to 1 P and 1 B ions) from previous publications.[26] The second site (−25.2 ppm) can be attributed to a Q^1_{2B} unit (a phosphate connected to 1 P and 2 B ions) due to its shielded chemical shift values and the low intensity one (−6.0 ppm) to a Q^0_{1B} species (a phosphate connected to 0 P and 1 B ions) due to its deshielded chemical shift values. Those three sites can be found in different proportions in the ^{31}P 2D map projections of samples with low MoO_3 amounts ($0 \leq x \leq 30$). At high MoO_3 amounts (x = 45−70), the ^{31}P projections can be decomposed

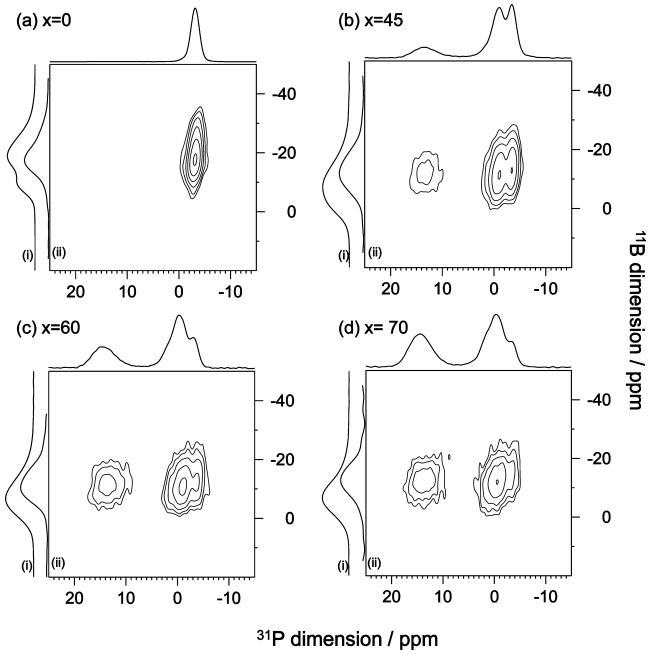

Figure 6. $^{11}B(^{31}P)$ D-HMQC 2D spectra of the x = 0 (a), 45 (b), 60 (c), and 70 (d) samples of the xMoO$_3$-(100-x)(50PbO-10B$_2$O$_3$-40P$_2$O$_5$) glass series. The 2D maps are displayed with the 1D ^{11}B MAS NMR as horizontal projection and with the 1D ^{31}P MAS NMR (i) and 2D maps projection (ii) along the vertical axis.

with two components at −11 and −20 ppm. While the first values could be assigned to a Q^0_{2B} species from previous publications,[26] the second chemical shift values is far from the values reported for the Q^0_{3B} or Q^0_{4B} units. Therefore, we propose that this Q^0 species also involved connection with Mo^{6+} groups. The presence of Mo^{6+} ions induces significant modifications of the chemical environment of the phosphate species leading to the unreported chemical shift values. In spite of its important place in the structural model (this species is the evidence of P/B/Mo mixing), its exact nature cannot be determined because the number of Mo^{6+} attached to that phosphate species (denoted as $Q^0_{B/Mo}$) cannot be determined from $^{31}P/^{95}Mo$ NMR correlation. Finally, all the NMR parameters (chemical shift, full width at half-maximum) have been determined and gathered in Table 2 (into brackets). This set of data has then been used as input parameters to decompose the 1D ^{31}P MAS NMR spectra of the complete composition line (Figure 7b). In the simulations, the components obtained from the 2D map projections are displayed in gray and the components that have to be added to obtain proper decompositions are displayed in white. These latter signals can thus be seen as signatures of phosphate groups not connected to any boron ions and are thus connected to either lead or Mo^{6+} ions. Among these "B-free" components, one signal (1.3 ppm) appears in addition to standards Q^3, Q^2, and Q^1 signals expected from the binary PbO−P$_2$O$_5$ system.[31] This signal, whom proportion increases with the MoO$_3$ content, has been assigned to a Q^0_{Mo} species in a good agreement with previous publications.[7] Finally, the correlation NMR technique indicates the presence of 9 different phosphate species all along the composition line. The NMR parameters of each signal (δ_{iso}, fwhm, and relative proportion) have been determined and reported in Table 2. The evolution of the phosphate network would be efficiently monitored by following the evolution of the different types of linkages that are POP, POB and POMo. Unfortunately, the uncomplete assignments of the $Q^0_{B/Mo}$ and the Q^0_{Mo} sites forbid these calculations. However, our NMR data can only be used to qualitatively discuss the network evolution by following the number of phosphate species involved in the three types of linkage. In this model, the P units involved in POP, POB and POMo linkages will be denoted as P_P (Q^3, Q^2, Q^1, Q^1_{1B}, Q^1_{2B}), P_B (Q^1_{1B}, Q^1_{2B}, Q^0_{1B}, Q^0_{2B}, and $Q^0_{B/Mo}$) and P_{Mo} ($Q^0_{B/Mo}$ and Q^0_{Mo}), respectively. Figure 8 presents the evolutions of the number of P atoms of the three types. It appears that insertion of MoO$_3$ reduces the number of P_P and increases the number of P_{Mo} units without changing significantly the P_B number. It is also noteworthy that below 30 mol % of MoO$_3$, the network is

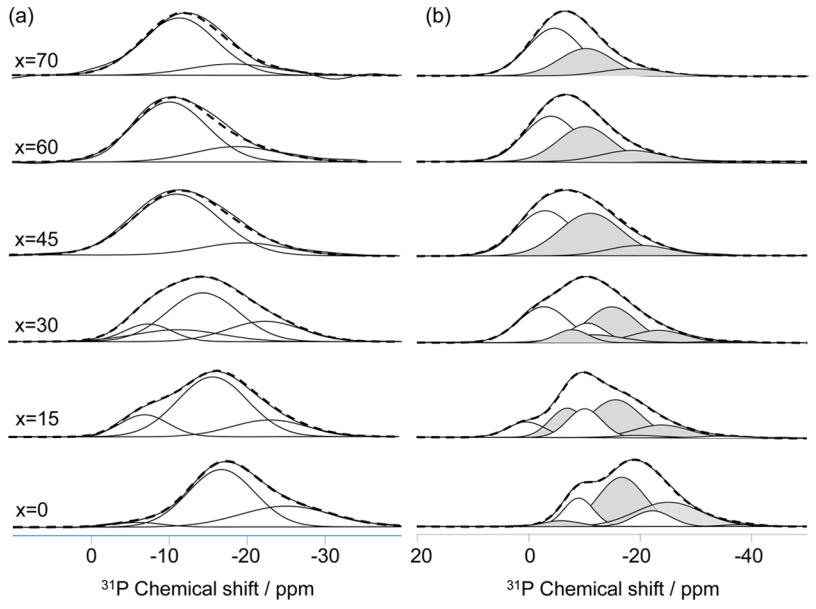

Figure 7. (a) ^{31}P projections of the 2D maps accompanied by the decompositions using a minimum number of components; (b) Decompositions of the 1D ^{31}P MAS NMR spectra with gray components corresponding to the signals determined from the 2D maps ^{31}P projections.

Table 2. ^{31}P NMR Parameters: Chemical Shift (δ_{iso}, ± 0.1 ppm), Full Width at Half Maximum (FWHM, ± 0.2 ppm) and Relative Proportions (Rel. Prop., ± 2%)[a]

MoO_3 (mol%)	Q^n	δ_{iso} (ppm)	fwhm (ppm)	rel. prop. (%)	Q^n	δ_{iso} (ppm)	fwhm (ppm)	rel. prop. (%)
0	Q^1_{2B}	−25.2 (−25.2)	14.0 (13.9)	28.5	Q^3	−38.0	7.7	1.5
	Q^1_{1B}	−16.8 (−16.8)	10.0 (10.1)	39.0	Q^2	−22.3	8.0	13.0
	Q^0_{1B}	−6.0 (−6.0)	7.8 (7.6)	3.5	Q^1	−9.1	6.3	14.5
5	Q^1_{2B}	−24.2	14.0	24.5	Q^3	−38.5	7.8	2.0
	Q^1_{1B}	−15.5	10.0	32.0	Q^2	−20.2	8.0	9.5
	Q^0_{1B}	−6.3	7.8	9.5	Q^1	−9.1	6.8	20.0
					Q^0_{Mo}	1.3	6.3	2.0
15	Q^1_{2B}	−23.9 (−23.4)	12.0 (11.5)	13.5	Q^3	−34.5	8.8	1.5
	Q^1_{1B}	−15.6 (−15.8)	10.5 (10.7)	34.5	Q^2	−20.0	8.5	4.5
	Q^0_{1B}	−6.9 (−7.0)	7.4 (7.3)	17.5	Q^1	−10.1	7.2	18.5
					Q^0_{Mo}	0.3	7.9	10.0
30	Q^1_{2B}	−23.4 (−22.5)	11.5 (11.3)	11.5	Q^3	−34.7	9.9	1.5
	Q^1_{1B}	−14.9 (−14.6)	10.6 (10.8)	28.5	Q^2	−19.7	10.8	2.0
	Q^0_{1B}	−7.8 (−7.5)	7.0 (7.2)	7.0	Q^1	−10.6	7.5	10.5
	Q^0_{2B}	−11.4 (−11.4)	13.0 (13.1)	11.5	Q^0_{Mo}	−2.7	10.6	27.5
45	Q^0_{2B}	−11.1 (−10.8)	13.1 (13.1)	46.0	Q^0_{Mo}	−2.9	11.8	42.0
	$Q^0_{B/Mo}$	−19.9 (−19.6)	13.0 (13.1)	12.0				
60	Q^0_{2B}	−10.3 (−10.2)	11.4 (11.2)	38.0	Q^0_{Mo}	−3.9	11.4	47.0
	$Q^0_{B/Mo}$	−18.6 (−18.7)	12.9 (13.0)	15.0				
70	Q^0_{2B}	−10.2 (−10.9)	11.3 (11.3)	33.0	Q^0_{Mo}	−4.5	11.3	57.0
	$Q^0_{B/Mo}$	−18.5 (−18.1)	12.8 (12.9)	10.0				

[a]The NMR parameters deduced from the simulations of the ^{31}P projections of the ^{11}B/^{31}P 2D maps are reported into brackets.

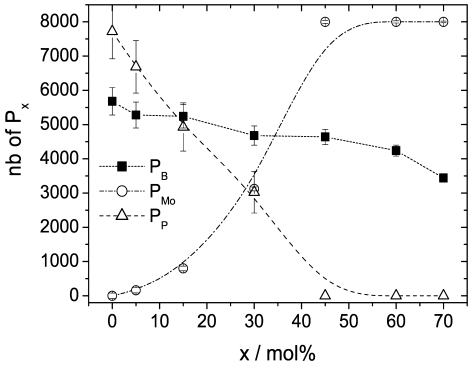

Figure 8. Evolutions of the number of P ions involved in POB (P_B), POMo (P_{Mo}), and POP (P_P) linkages deduced from the decompositions of the ^{31}P MAS NMR spectra.

mainly composed by P_B and P_P atoms, whereas P_B and P_{Mo} dominate for MoO_3 contents above 30 mol %.

3.4. Continuous Wave EPR Characterization. The EPR spectra of the glasses series are presented in Figure 9. All the spectra show a weak hyperfine structure with six lines in both parallel ($g_\parallel$) and perpendicular ($g_\perp$) bands. These may be attributed to the 5/2 nuclear spin of ^{95}Mo (15.9%) and ^{97}Mo (9.6%). The intense central absorption line belongs to the ^{96}Mo isotope (74.5%) which has a nuclear spin $I = 0$. Depending on the symmetry of the molybdenum paramagnetic site, the g and A tensor are anisotropic. The different glasses have an axial symmetry with the principal values $g_{zz} = g_\parallel \cong 1.895$ (orientation of the external magnetic field parallel to the magnetic z-axis) and $g_{xx} = g_{yy} = g_\perp \cong 1.930$ (orientation of the external magnetic field perpendicular to the magnetic z-axis) where $g_\perp > g_\parallel$. Similar results can be obtained for the hyperfine tensor: $A_{zz} = A_\parallel \cong 100.10^{-4}$ cm^{-1}; $A_{xx} = A_{yy} = A_\perp \cong 50.\ 10^{-4}$ cm^{-1} where $A_\perp < A_\parallel$. The characteristic EPR parameters are gathered in Table 3. These experimental EPR values indicate an axially compressed 6-coordinated environment for the Mo^{5+} ions.[32,33] The partial disappearance of the hyperfine structure is observed with the increase of MoO_3 concentration (Figure 9), due to the dipolar interaction between the Mo^{5+} ions. From the

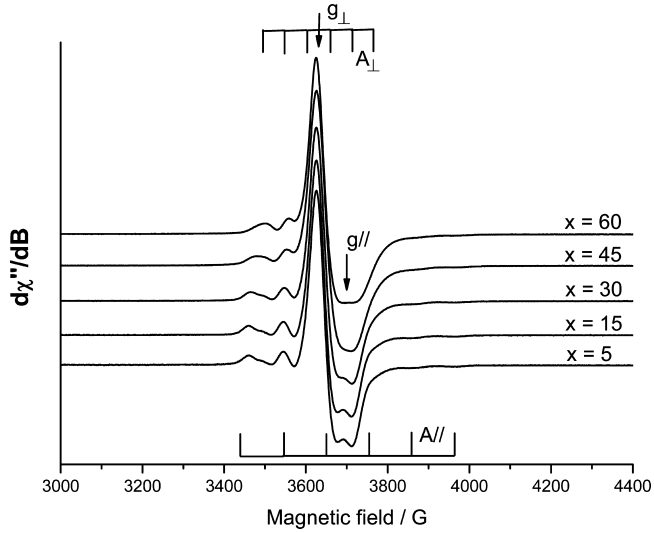

Figure 9. CW EPR spectra recorded at room temperature of the xMoO$_3$-(100-x)(50PbO-10B$_2$O$_3$-40P$_2$O$_5$) glass series.

Table 3. EPR Parameters of Mo^{5+} Ions in the xMoO$_3$-(100-x)(50PbO-10B$_2$O$_3$-40P$_2$O$_5$) Glass Series[a]

x (mol %)	$g_\parallel$	$A_\parallel$ (cm^{-1})	$g_\perp$	$A_\perp$ (cm^{-1})
5	1.898	102	1.931	51.10^{-4}
15	1.897	100	1.930	51.10^{-4}
45	1.895	100	1.933	52.10^{-4}
60	1.896	102	1.934	52.10^{-4}

[a]$g_\parallel$ and $g_\perp$ are given with error of ±0.001 and $A_\parallel$ and $A_\perp$ with error of 1.10^{-4}.

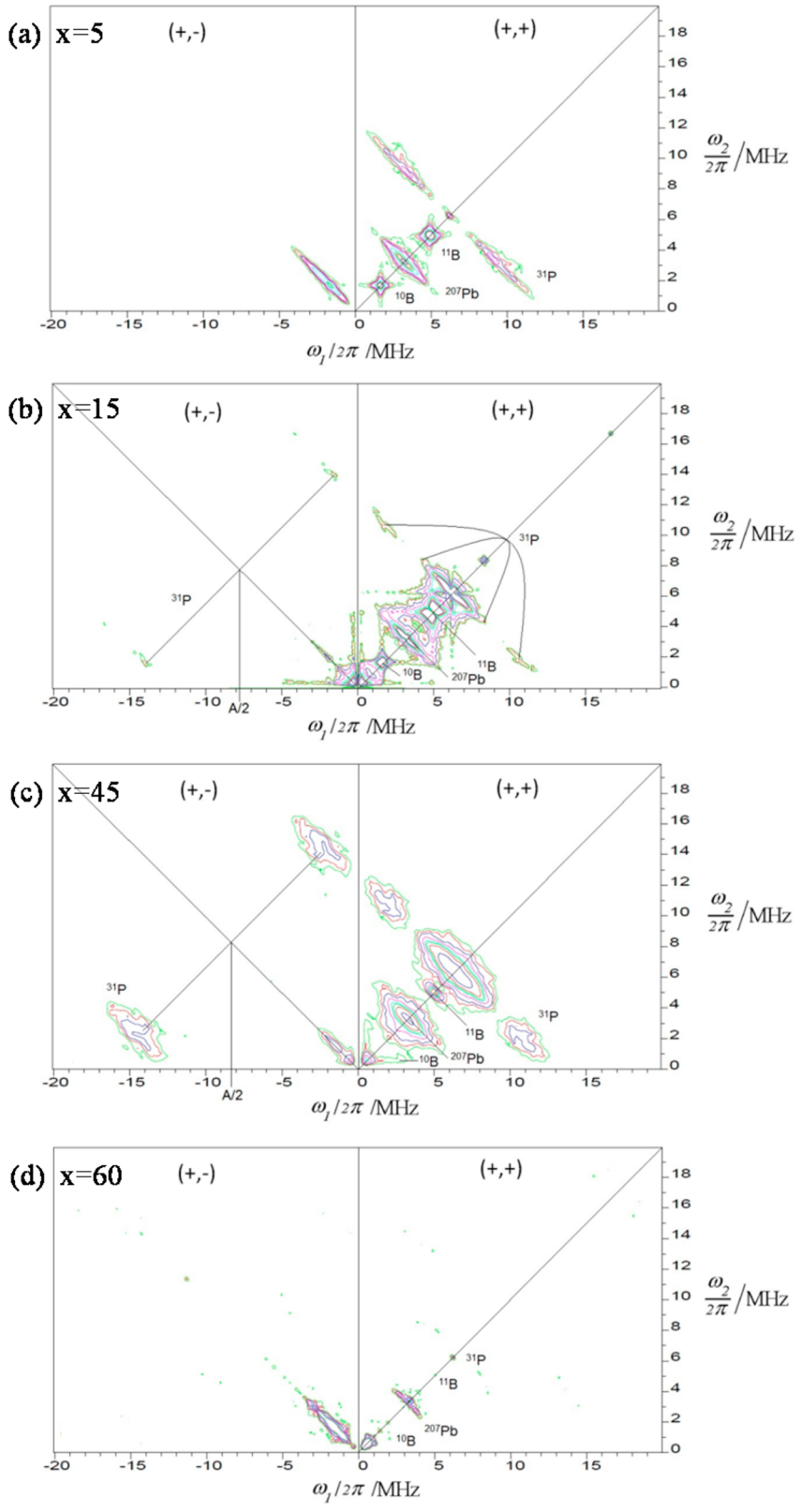

Figure 10. Two-dimensional HYSCORE spectra recorded at 5 K of the x = 5 (a), 15 (b), 45 (c), and 60 (d) samples of the xMoO$_3$-(100-x)(50PbO-10B$_2$O$_3$-40P$_2$O$_5$) glass series.

quantification of the EPR spectra, it has been shown that our glasses contain a very low amounts of reduced molybdenum ions (<1% of total Mo), as previously reported in similar glass systems.[7,34]

3.5. Pulsed EPR Characterization. In order to go further in the description of the local nuclear environment of the Mo^{5+} centers, pulsed EPR experiments were performed using two-dimensional HYSCORE experiments to get information on the

nuclear environments of Mo^{5+} and to determine the hyperfine couplings. At low MoO_3 content ($x = 5$), the spectrum (Figure 10a) shows in the (+,+) quadrant a pair of cross peaks centered at 1.60, 4.78, 3.13, and 6.03 MHz corresponding to ^{10}B, ^{11}B, ^{207}Pb, and ^{31}P nuclear Larmor frequencies, respectively. The hyperfine coupling constants A values measured for ^{31}P and ^{207}Pb are respectively 11 and 3.5 MHz. These couplings A are partially composed of a contribution related to the electron delocalization over the coupled nuclei, i.e., Fermi contact term, and another contribution from the orbital recovering with the dipolar part of the A tensor. The flat ridge observed arises mainly from Fermi contact term coupling. Only diagonal nuclear Larmor frequencies were observed for ^{10}B and ^{11}B resulting in nonmeasurable hyperfine couplings. No strong coupling is observed in (+,−) quadrant. At $x = 15$, the 2D HYSCORE spectrum (Figure 10b) shows a more complex feature. In the (+,−) quadrant a pair of cross peaks arising for the strong coupling case ($A > 2\nu(^{31}P)$) can be observed. The cross peaks are separated by 12.6 MHz (twice the ^{31}P nuclear frequency) and split at $A/2$. The A determined from experimental spectrum is 16 MHz. In the (+,+) quadrant are observed a pair of two cross peaks due to ^{31}P associated with a weak coupling of 5 and 11 MHz. Weak couplings are also observed with ^{10}B, ^{11}B and ^{207}Pb ($A = 3.5$ MHz) nuclei. The HYSCORE spectrum of the $x = 45$ sample (Figure 10c) displays a pair of cross peaks in the (+,−) quadrant arising for the strong coupling case ($A > 2\nu(^{31}P)$) as previously observed in case of the $x = 15$ sample. The A determined from the experimental spectrum is 16 MHz. Two other cross peaks are also observed for ^{31}P in the (+,+) quadrant with weak coupling constants (5 and 11 MHz, respectively). Weak couplings are also observed for ^{10}B, ^{11}B, and ^{207}Pb ($A = 3.9$ MHz) nuclei. The hyperfine tensor A has principal values (A_{xx}, A_{yy}, A_{zz}). In the point-dipole approximations, it can be written in the form ($A_{iso}-T$, $A_{iso}-T$, $A_{iso}+2T$) where A_{iso} is the isotropic hyperfine coupling constant and the dipolar hyperfine tensor is $T = g_e g_n \beta_n \beta_e / h^3$, where r is the effective electron−nucleus distance.[35] The individual shape of the ridges depends on the magnitude of the dipolar hyperfine coupling constant. The larger is T, the more expanded are the ridges. At $x = 45$, the hyperfine tensor A is mainly dominated by the dipolar part T, which can be roughly estimated from the maximum vertical shifts of the ridge of Figure 10c that yield to $T^{Pb} = 1.9 \pm 0.1$ MHz and $T^{P} = 2.2 \pm 0.1$ MHz that corresponds, respectively, to a distance of the unpaired electron of 0.35 ± 0.02 nm and 0.33 ± 0.02 nm. Regarding the solid at $x = 60$ mol % MoO_3 (Figure 10d), a drastic change is observed with the disappearance of couplings with the different nuclei.

4. DISCUSSION

The impact of Mo ions insertion in the glass matrix has been monitored using magnetic resonance spectroscopies in order to understand how the molybdate species enter into the network and change the glass structure. The NMR investigation shows that MoO_3 strongly impacts the borophosphate network structure. All along the composition line, four different borate and nine different phosphate units have been identified, whereas ^{95}Mo NMR does not permit to identify more than one single Mo^{6+} species. With increasing MoO_3 content, the NMR data indicate an evolution from 4-coordinated units to 3-coordinated borate units and a progressive depolymerization of the phosphate network from Q^2 units to Q^1 and Q^0 connected to B^{3+} and Mo^{6+} ions. While all these structural modifications have already been observed in several borophosphate systems,[22−24,26,27] it is noteworthy that our system presents a constant P/B ratio all along the composition line whereas previous investigated systems involved various B/P values, coming from a B/P substitution or a B_2O_3 addition in a constant P_2O_5 formulation. Therefore, the B/P ratio, which is usually considered as a key parameter to explain the structural modifications, cannot be directly used in our study. At low amounts (0−15 mol %), ^{31}P NMR shows that Mo^{6+} ions preferentially interact with the phosphate entities not connected to any boron (Q^2 and Q^1) to create phosphate species surrounded by Mo ions, as shown by the decrease of P_P units and the simultaneous increase of P_{Mo} in Figure 8. Within this region, the borophosphate network is slightly affected, as shown by the small decrease of the P_B number (Figure 8) but also by the almost constant relative proportions of Q^1_{2B}, Q^1_{1B}, and Q^0_{1B} species (Table 2). However, the small decrease of P_B corresponds to a slight extraction of P from the borophosphate network, resulting in an artificial increase of the B/P ratio concerning the borophosphate network. This modification is in line with the decrease of $B^{IV}_{(1)}$ and increase of $B^{IV}_{(2)}$ observed in Figure 4 within the 0−15 mol % region and the appearance of B^{III} signal in the 15−30 mol % region. The $x = 30$ composition can be considered as a critical formulation because of the numerous modifications appearing for that composition: (i) from a qualitative point of view, a new P_B site appears corresponding to a Q^0_{2B} species, indicating that the nature of the borophosphate species is affected by the Mo^{6+} insertion (Table 2); (ii) quantitatively, the increasing P_{Mo} number is now equal to the decreasing P_P number showing that the glass network is shifting from a "P_P + P_B" to a "P_B + P_{Mo}" nature (Figure 8); and (iii) Mo^{6+} chemical environment changes as shown by the increase of the signal width in Figure 2. If this broadness increase cannot be fully interpreted, then we can assume that a new structural feature like a new linkage (BOMo or MoOMo) could be at the origin of this evolution. At high MoO_3 amounts ($x > 30$ mol %), Mo^{6+} ions directly react with the borophosphate units to create the $Q^0_{B/Mo}$ species, showing that the association between the three elements (Table 2) occurs within the glass structure. The phosphate network is now dominated by P_{Mo} units rather than P_B, P_P sites having decreased down to 0. It is also noteworthy that all the phosphate units are now connected to Mo^{6+} ions, as shown by the plateau in Figure 8 corresponding to the total number of P of the formulation. Within this region, the borate speciation also evolves with a clear increase of $B^{IV}_{(3)}$ and B^{III} units at the expense of $B^{IV}_{(1)}$ and $B^{IV}_{(2)}$ groups. We propose that $B^{IV}_{(3)}$ results from reactivity between the borate and the molybdate species. Indeed, we believe that, after having reacted with all the P^{5+} ions, Mo^{6+} ions interact with borate units with a preference toward B^{IV} sites leading to the formation of the $B^{IV}_{(3)}$ groups. This reactivity could explain the loss of BOB connectivity observed in the 2D $^{11}B/^{11}B$ map (Figure 5d) through the B^{IV}/B^{IV} and B^{IV}/B^{III} signals disappearance. Altogether, all this structural modification can be used to understand the two-domain evolution of the macroscopic property of T_g. At low MoO_3 amounts (<30 mol %), molybdenum insertion leads to a T_g increase because of the creation of POMo linkages that strengthen the glass network. At higher MoO_3 amounts (>30 mol %), the number of PMo reaches a maximum amount and can no longer contribute to the T_g increase. Moreover, the new structural features like tricoordinated borate and/or B—O—

Mo linkage are created. We believe that planar B^{III} and BOMo linkages do not contribute to the previously observed strengthening but induce a global weakening of the glass network resulting in the T_g decrease noticed in Figure 1.

In spite of its low amount (<1%), the influence of Mo^{5+} on glasses structure has also been investigated by CW and pulsed EPR spectroscopy. The CW spectra are characteristic of Mo^{5+} in axial symmetry with $g_\perp > g_\parallel$. While the local geometry is not affected by the MoO_3 amount, pulsed 2D-HYSCORE spectra show a clear difference in the Mo^{5+} local chemical environment. At low and intermediate amounts (5−45 mol %), the Mo^{5+} ions are weakly coupled with two types of phosphorus (A = 5 and 11 MHz) and strongly with one type of phosphorus (A = 16 MHz), indicating that Mo^{5+} ions are located in the very close vicinity of the phosphate network. At x = 60 mol % MoO_3, a clear change can be observed in the HYSCORE spectrum through the coupling disappearance with all elements (^{31}P, ^{10}B, ^{11}B, ^{207}Pb), indicating that the Mo^{5+} ions are not close to the glass network units.

5. CONCLUSIONS

The impact of MoO_3 insertion in the mixed borophosphate network structure has been analyzed for the first time using magnetic resonance spectroscopies. 1D/2D MAS NMR indicates significant evolution of the glass network through the identification of 4 borate and 9 phosphate species all along the composition line. Moreover, NMR provided unreported insights on the molybdenum insertion mechanism. It turned out that Mo^{6+} ions interacts (i) with "boron free"-P atoms in a first time to create P—O—Mo linkages outside of the borophosphate network, (ii) with the borophosphate units in a second time to create structural units involving the three element ($Q^0_{B/Mo}$), and (iii) with the tetra-coordinated borate units in a third time to finally create "isolated" B^{IV} groups. Even if the evolution of POP, POB, and POMo linkage cannot be determined (due to the uncompleted assignment of the $Q^0_{B/Mo}$ and Q^0_{Mo} phosphate units), a qualitative model has been used to explain the two-domains evolution of T_g. In the low MoO_3 amounts (0−30 mol %), replacement of POP by POMo linkage strengthens the network and induces a T_g increase, whereas in the high Mo_3 amounts, formation of BOMo bonds and appearance of B^{III} groups induce a global weakening of the network, leading to a T_g decrease. The CW EPR technique has shown that the proportion of reduced molybdenum is <1% and that Mo^{5+} adopts an axially compressed 6-coordinated position. HYSCORE experiments indicate that Mo^{5+} ions are close to P ions at low MoO_3 amounts, these interaction disappearing at higher MoO_3 contents.

AUTHOR INFORMATION

Corresponding Author

*Phone: +33 320434332. E-mail: gregory.tricot@univ-lille1.fr (G.T.).

Notes

The authors declare no competing financial interest.

ACKNOWLEDGMENTS

The French authors would like to thank Region Nord Pas de Calais, Europe (FEDER), CNRS, University of Lille, and TGIR-RMN-THC FR3050 CNRS for funding. The Czech authors are grateful for the financial support from the project No. 13-00355S of the Grant Agency of the Czech Republic.

REFERENCES

(1) Van Wazer, J. R. *Phosphorus and Its Compounds*; Interscience Publishers: New York/London, 1958.

(2) Duffy, J. A.; Ingram, M. D. An Interpretation of Glass Chemistry in Terms of the Optical Basicity Concept. *J. Non-Cryst. Solids* **1976**, *21*, 373−410.

(3) Magnin, M.; Schuller, S.; Caurant, D.; Majerus, O.; De Ligny, D.; Mercier, C. Effects of Compositional Changes on the Structure and Crystallization Tendency of a Borosilicate Glass Containing MoO_3. *Ceram. Trans.* **2009**, *207*, 59−68.

(4) Schuller, S.; Pinet, O.; Penelon, B. Liquid-liquid Phase Separation Process in Borosilicate Liquids Enriched in Molydbenum and Phosphate Oxides. *J. Am. Ceram. Soc.* **2011**, *94*, 447−454.

(5) Hekmat-Shoar, M. H.; Hogarth, C. A.; Moridi, G. R. A Study of the Electrical Properties of Molybdenum Phosphate Glasses. *J. Mater. Sci.* **1985**, *20*, 889−894.

(6) Toloman, D.; Ciceo-Lucacel, R.; Magdas, D. A.; Regos, A.; Biris, A.-R.; Leostean, C.; Ardelean, I. The Modifier/former Role of MoO_3 in some Calcium-phosphate Glasses. *J. Alloys Compd.* **2013**, *556*, 67−70.

(7) Subcik, J.; Koudelka, L.; Mosner, P.; Montagne, L.; Tricot, G.; Delevoye, L.; Gregora, I. Glass-forming ability and structure of ZnO-MoO_3-P_2O_5 glasses. *J. Non-Cryst. Solids* **2010**, *356*, 2509−2516.

(8) Ottoboni, F. S.; Poirier, G.; Cassanjes, F. C.; Messaddeq, Y.; Ribeiro, S. J. L. Crystallization Study of Molybdate Phosphate Glasses by Thermal Analysis. *J. Non-Cryst. Solids* **2009**, *355*, 2279−2284.

(9) Santagnelli, S. H.; De Araujo, C. C.; Strojek, W.; Eckert, H.; Poirier, G.; Ribeiro, S. J. L.; Messaddeq, Y. Structural Studies of $NaPO_3$-MoO_3 Glasses by Solid-state Nuclear Magnetic Resonance and Raman Spectroscopy. *J. Phys. Chem. B* **2007**, *111*, 10109−10117.

(10) Subcik, J.; Koudelka, L.; Mosner, P.; Cernosek, Z. Zinc Borophosphate Glasses Doped with Molydenum Oxide. *Adv. Mater. Res.* **2008**, *39*−*40*, 97−100.

(11) Subcik, J.; Koudelka, L.; Mosner, P.; Montagne, L.; Gregora, I. Structure and Properties of MoO_3-containing Zinc Borophosphate Glasses. *J. Non-Cryst. Solids* **2009**, *355*, 970−975.

(12) Koudelka, L.; Rosslerova, I.; Cernosek, Z.; Mosner, P.; Montagne, L.; Revel, B.; Tricot, G. Structure and properties of lead borophosphate glasses doped with molybdenum oxide. *Phys. Chem. Glasses: Eur. J. Glass. Sci. Technol. B* **2012**, *53*, 245−253.

(13) Rosslerova, I.; Koudelka, L.; Holubova, J.; Mosner, P.; Montagne, L.; Revel, B. Investigation of (100-x)[0.5PbO-0.2B_2O_3-0.3P_2O_5]-MoO_3 glasses. *Phys. Chem. Glasses: Eur. J. Glass Sci. Technol., Part B* **2015**, *46*, 1−7.

(14) Carr, H. Y.; Purcell, E. M. Effects of Diffusion on Free Precession in Nuclear Magnetic Resonance Experiments. *Phys. Rev.* **1954**, *94*, 630−638.

(15) Larsen, F. H.; Jakobsen, H. J.; Ellis, P. D.; Nielsen, N. C. QCPMG-MAS NMR of Half Integer Quadrupolar Nuclei. *J. Magn. Reson.* **1998**, *131*, 144−147.

(16) Gan, Z. $^{13}C/^{14}N$ Heteronuclear Multiple Quantum Correlation with Rotary Resonance and REDOR Dipolar Recoupling. *J. Magn. Reson.* **2007**, *184*, 39−43.

(17) Tricot, G.; Trébosc, J.; Pourpoint, F.; Gauvin, R.; Delevoye, L. The DHMQC MAS-NMR Technique: An Efficient Tool for the Editing of Through-Space Correlation Spectra Between Quadrupolar and Spin = 1/2 (^{31}P, ^{29}Si, ^{1}H, ^{13}C) Nuclei. *Ann. Rep. Nucl. Magn. Reson. Spectr.* **2013**, *81*, 145−184.

(18) Wang, Q.; Hu, B.; Lafon, O.; Trebosc, J.; Deng, F.; Amoureux, J.-P. Double-Quantum Homonuclear NMR Correlation Spectroscopy of Quadrupolar Nuclei Subjected to Magic-Angle Spinning and High Magnetic Field. *J. Magn. Reson.* **2009**, *200*, 251−260.

(19) Brinkmann, A.; Kentgens, A. P. M. Proton Selective ^{17}O-^{1}H Distance Measurements in Fast Magic Angle Spinning Solid State NMR Spectroscopy for the Determination of Hydrogen Bond Lenghts. *J. Am. Chem. Soc.* **2006**, *128*, 14758−14759.

(20) Tricot, G.; Raguenet, B.; Silly, G.; Ribes, M.; Pradel, A.; Eckert, H. P-O-B^3 Linkages in Borophosphate Glasses Evidenced by High

Field $^{11}B/^{31}P$ Correlation NMR. *Chem. Commun.* **2015**, *51*, 9284−9286.
(21) Höfer, P.; Grupp, A.; Nebenfürh, H.; Mehring, M. Hyperfine sublevel correlation (HYSCORE) spectroscopy: A 2D ESR investigation of the squaric acid radical. *Chem. Phys. Lett.* **1986**, *132*, 279−282.
(22) Schweiger, A.; Jeschke, G. *Principle of Pulsed Electron Paramagnetic Resonance*; Oxford University Press: Oxford, U.K., 2001.
(23) Raskar, D.; Rinke, M. T.; Eckert, H. The Mixed-network Former Effect in Phopshate Glasses: NMR and XPS Studies of the Connectivity Distribution in the Glass System $(NaPO_3)_{1-x}B_2O_3x$. *J. Phys. Chem. C* **2008**, *112*, 12530−12539.
(24) Larink, D.; Eckert, H.; Reichert, M.; Martin, S. W. Mixed Network Former Effect in Ion-conducting Alkali Borophosphate Glasses: Structure/Properties Correlations in the System $[M_2O]_{1/3}[(B_2O_3x(P_2O_5)_{1-x}]_{2/3}$ (M = Li,K,Cs). *J. Phys. Chem. C* **2012**, *116*, 26162−26176.
(25) Funke, L.-M.; Eckert, H. Charge Compensation in Sodium Borophosphate Glasses Studied by $^{11}B(^{23}Na)$ and $^{31}P(^{23}Na)$ Rotational Echo Double Resonance Spectroscopy. *J. Phys. Chem. C* **2016**, *120*, 3196−3205.
(26) Raguenet, B.; Tricot, G.; Silly, G.; Ribes, M.; Pradel, A. Revisiting the 'mixed glass former effect' in ultra-fast quenched borophosphate glasses by advanced 1D/2D solid state NMR. *J. Mater. Chem.* **2011**, *21*, 17693−17704.
(27) Tricot, G.; Saitoh, A.; Takebe, H. Intermediate length scale organization in tin borophosphate glasses: new insights from high field correlation NMR. *Phys. Chem. Chem. Phys.* **2015**, *17*, 29531−29540.
(28) Massiot, D.; Fayon, F.; Capron, M.; King, I.; Le Calvé, S.; Alonso, B.; Durand, J. O.; Bujoli, B.; Gan, Z.; Hoaston, G. Modelling One and Two- Dimensional Solid-state NMR Spectra. *Magn. Reson. Chem.* **2002**, *40*, 70−76.
(29) Brow, R. K.; Kirckpatrick, R. J.; Turner, G. L. Nature of Alumina in Phosphate Glass: II, Structure of Sodium Aluminophosphate Glass. *J. Am. Ceram. Soc.* **1993**, *76*, 919−928.
(30) Van Wüllen, L.; Wenger, S.; Tricot, G. An Advanced NMR Protocol for the Structural Charactrization of Aluminophosphate Glasses. *Solid State Nucl. Magn. Reson.* **2007**, *32*, 44−52.
(31) Fayon, F.; Bessada, C.; Coutures, J.-P.; Massiot, D. High-resolution Double Quantum ^{31}P MAS NMR Study of the Intermediate-range Order in Crystalline and Glass Lead Phosphates. *Inorg. Chem.* **1999**, *38*, 5212−5218.
(32) Cozar, O.; Magdas, D. A.; Ardelean, I. EPR study of molybdenum-lead-phosphate glasses. *J. Non-Cryst. Solids* **2008**, *354*, 1032−1035.
(33) Lakshmana Rao, B.; Ravi Babu, Y.N.Ch.; Prasad, S.V.G.V.A. Spectroscopic and EPR studies on $PbO-Y_2O_3-P_2O_5$ glasses doped with molybdenum ion. *Phys. B* **2013**, *429*, 68−72.
(34) Boudlich, D.; Haddad, M.; Nadiri, A.; Berger, R.; Kliava, J. Mo^{5+} ions as EPR structural probes in molybdenum phosphate glasses. *J. Non-Cryst. Solids* **1998**, *224*, 135−142.
(35) Dikanov, S. A.; Tsvetkov, Y. D. *ESEEM Spectroscopy*; CRC: London, 1992.